Check for updates

Integrated optical frequency comb technologies

Lin Chang [1 ✉], Songtao Liu [1,2] and John E. Bowers [1 ✉]

Optical frequency combs offer an unrivalled degree of frequency measurement precision that underpins the advance of modern technology in both fundamental science and commercial contexts. Recent progress in integrated photonics provides an attractive route to realize optical frequency comb sources in a compact, low-cost and energy-efficient manner by leveraging tightly-confined waveguide platforms and wafer-scale mass-manufacturing in photonic foundries, potentially revolutionizing the fields of information processing, time–frequency metrology and sensing. In this Review Article, we comprehensively examine the strategies for optical frequency comb generation in integrated photonics and provide detailed appraisals of those strategies in the context of prospective applications. The progress of high-level integration of optical frequency combs in photonic integrated circuits is summarized and a roadmap is proposed for transferring advanced optical frequency comb systems from the laboratory to the wider world.

Nearly 60 years after the invention of the mode-locked laser (MLL)[1], optical frequency combs (OFCs) have evolved into one of the most active areas in photonics. Although the term 'optical frequency comb' originally referred to only self-referenced combs in timekeeping experiments, its use has since expanded to include all light sources whose spectra consist of discrete, equally spaced frequency lines[2]. Nowadays, OFCs have also found a much broader application space: in communications, a single comb source can provide tens to thousands of optical frequency lines for massive parallelization in wavelength-division multiplexed (WDM) systems and thus address the rapid growth of data traffic in the Internet and data centres[3,4]. In time–frequency metrology, OFCs have proved to be a remarkable tool for coherently bridging optical frequencies in hundreds of terahertz (THz) and electronically accessible frequencies within hundreds of gigahertz (GHz). This capability is invaluable for applications such as optical spectroscopy, optical frequency synthesizers and timekeeping[5]. For example, the most accurate atomic clock in the world, which has a relative frequency inaccuracy of below 10^{-18}, relies on OFCs to count the optical oscillations and down-convert to detectable radio frequencies (RFs)[6,7].

Despite their clear value and importance, OFC-based technologies were mainly deployed in research laboratories because they usually depended on bulky, power-hungry, expensive equipment to generate, control and manipulate the comb light. Over the past two decades, the blooming of integrated photonics, particularly silicon-based integrated photonics, has allowed the production of OFC devices through the use of advanced lithography and nanofabrication techniques[8]. By leveraging modern manufacturing infrastructure, integrated photonics offers great advantages in lowering the system size, weight and power consumption, and cost (SWaP-C)[9]. Therefore, it holds the potential to accelerate the transition of OFCs from research laboratory experiments to consumer applications, including many emerging technologies, such as autonomous driving[10], 5G/6G communications[11] and machine learning[12,13].

So far, remarkable achievements have been made in the development of OFCs in integrated photonics[8]. Various approaches for enabling comb generation on-chip have emerged on different photonic platforms, whose performance in many aspects, such as the comb span[14,15] and noise[16], is now comparable to traditional solid-state or fibre-based comb sources. Over the past few years, efforts to combine OFCs with other photonic components have facilitated a number of system-level demonstrations[17,18]. Although relatively new, this area has already delivered a wide range of advanced technologies that extend the capabilities of integrated photonics.

In this article, we review the history, rapid progress, current status and future of integrated OFC technologies. We first give a device-level examination of the two main categories of comb sources in integrated photonics: semiconductor mode-locked lasers (SMLLs) and nonlinear frequency combs. Different comb-generating strategies are compared using key metrics within the context of prospective applications. Next, at the system level, we summarize the growing efforts and recent advances in higher-level integration between OFCs and other photonic components. Furthermore, we discuss the challenges and opportunities of bringing OFCs into fully integrated photonic circuits and realizing high-volume production in photonic foundries in the future.

Integrated semiconductor mode-locked lasers

MLLs are a special class of lasers that output coherent combs with all of the longitudinal modes phase-locked and equally spaced in the frequency domain[19]. Solid-state-based and fibre-based MLLs have achieved great success, but are inappropriate for cost-sensitive and energy-consumption-sensitive applications like telecommunications. To meet these needs, integrated solutions can offer a high wall plug efficiency (WPE), small footprint and mass-production capability. The historical evolution of integrated MLLs is sketched in the lower part of Fig. 1. Here we focus on SMLLs, the dominant approach for realizing MLLs on photonic chips.

Mode-locking mechanism. *Active mode locking.* Mode-locked behaviour can be realized by applying an electrical modulation signal to the gain section or an optical modulator within the laser cavity[20] (Fig. 2a). At the modulation frequency close to the cavity roundtrip frequency (or one of the higher harmonics), the gain section/modulator's modulation bandwidth (usually determined by the parasitic capacitance and resistance) should be large enough to enable efficient modulation. To get short optical pulses from the device, the RF signal must be stable and have a large amplitude,

[1]Department of Electrical and Computer Engineering, University of California, Santa Barbara, CA, USA. [2]Present address: Intel Corporation, Santa Clara, CA, USA. ✉e-mail: linchang@ece.ucsb.edu; bowers@ece.ucsb.edu
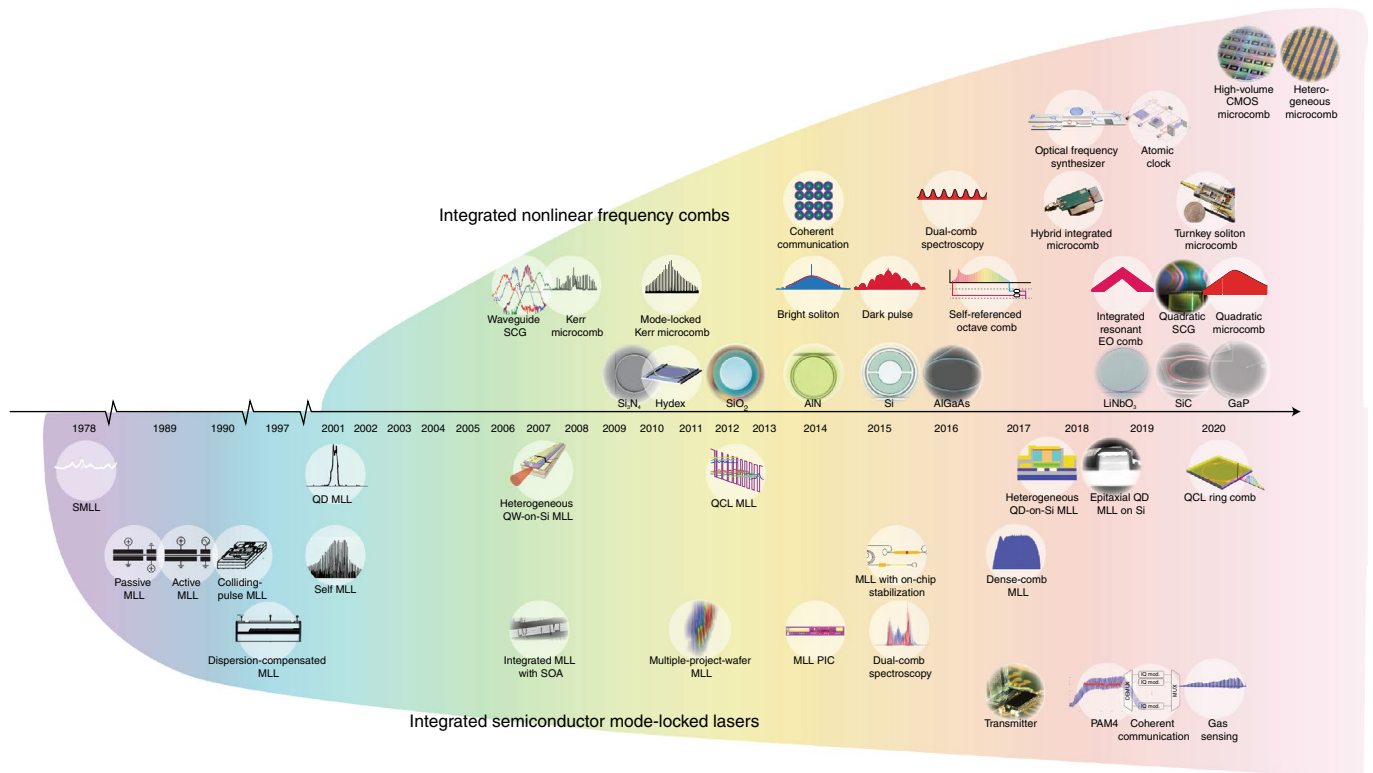
Fig. 1 | Timeline of the evolution of integrated OFC technologies. Upper half: integrated nonlinear OFCs, from lower to higher rows (with increasing integration level and complexity). Platform: Si_3N_4 (ref. [62]), Hydex[64], SiO_2 (refs. [63,136]), AlN[67], Si[65], AlGaAs[66], $LiNbO_3$ (ref. [69]), SiC[71] and GaP[68]. Device-level demonstration/phenomenon observation: waveguide SCG[44], Kerr microcomb[43], mode-locked Kerr microcomb[56], bright soliton[137], dark pulse[60], self-referenced comb[51,138], integrated resonant EO comb[83,139], quadratic SCG[15] and microcomb[88]. System-level demonstration/high-level integration: coherent communication[140], dual-comb spectroscopy[141], atomic clock[18], optical frequency synthesizer[17], hybrid integrated microcomb[127], turnkey soliton microcomb[111], high-volume CMOS microcomb[16] and heterogeneous laser-soliton micrcomb[122]. Lower half: integrated SMLLs, from higher to lower rows (with increasing integration level and complexity). Platform: SMLL[142], QD MLL[143], heterogeneous QW-on-Si MLL[144], QCL MLL[27], heterogeneous QD-on-Si MLL[25] and epitaxial QD MLL grown on Si[26]. Device-level demonstration/phenomenon observation: passive MLL[145], active MLL[31], colliding-pulse MLL[146], self MLL[147], MLL with on-chip stabilization[134], dense-comb MLL[93] and QCL ring comb[148]. System-level demonstration/high-level integration: dispersion-compensated MLL[149], integrated MLL with SOA[150], multiple-project-wafer MLL[151], MLL PIC[152], dual-comb spectroscopy[153], transmitter[131], Pulse Amplitude Modulation 4-level (PAM4) (ref. [41]), coherent communication[154] and gas sensing[155]. Images adapted with permission from: Si_3N_4, ref. [62], Springer Nature Ltd; Hydex, ref. [64], Springer Nature Ltd; SiO_2, refs. [63,136], APS and Springer Nature Ltd; AlN, ref. [67], OSA; Si, ref. [65], Springer Nature Ltd; AlGaAs, ref. [66], OSA; $LiNbO_3$, ref. [69], OSA; SiC, ref. [71], OSA; GaP, ref. [68], Springer Nature Ltd; waveguide SCG, ref. [44], OSA; Kerr microcomb, ref. [43], Springer Nature Ltd; mode-locked Kerr microcomb, ref. [56], Springer Nature Ltd; bright soliton, ref. [137], Springer Nature Ltd; dark pulse, ref. [60], Springer Nature Ltd; self-referenced comb, refs. [51,138], Springer Nature Ltd; integrated resonant EO comb, refs. [83,139], Springer Nature Ltd; quadratic SCG, ref. [15], OSA; quadratic microcomb, ref. [88], Springer Nature Ltd; coherent communication, ref. [140], Springer Nature Ltd; dual-comb spectroscopy, ref. [141], AAAS; atomic clock, ref. [18], OSA; optical frequency synthesizer, ref. [17], Springer Nature Ltd; hybrid integrated microcomb, ref. [127], Springer Nature Ltd; turnkey soliton microcomb, ref. [111], Springer Nature Ltd; high-volume CMOS microcomb, ref. [16], Springer Nature Ltd; heterogeneous laser-soliton microcomb, ref. [122], AAAS; SMLL, ref. [142], American Institute of Physics; QD MLL, ref. [143], American Institute of Physics; heterogeneous QW-on-Si MLL, ref. [144], OSA; QCL MLL, ref. [27], Springer Nature Ltd; heterogeneous QD-on-Si MLL, ref. [25], IEEE; epitaxial QD MLL grown on Si, ref. [26], Wiley; passive MLL, ref. [145], American Institute of Physics; active MLL, ref. [31], Wiley; colliding-pulse MLL, ref. [146], American Institute of Physics; self MLL, ref. [147], Wiley; MLL with on-chip stabilization, ref. [134], IEEE; dense-comb MLL, ref. [93], Springer Nature Ltd; QCL ring comb, ref. [148], OSA; dispersion-compensated MLL, ref. [149], IEEE; integrated MLL with SOA, ref. [150], IEEE; multiple-project-wafer MLL, ref. [151], OSA; MLL PIC, ref. [152], OSA; dual-comb spectroscopy, ref. [153], American Institute of Physics; transmitter, ref. [131], Springer Nature Ltd; PAM4, ref. [41], OSA; coherent communication, ref. [154], OSA; gas sensing, ref. [155], OSA.

which creates a short time window of net gain (Fig. 2b). In operation, each of the non-equidistant longitudinal modes within the laser cavity will acquire an equidistant modulation sideband. Since these sidebands are very close to the adjacent cavity modes, all of the lasing modes tend to couple together by the frequency pulling effect, leading to a mode-locked state (Fig. 2c)[21].

Passive mode locking. Passive mode locking is currently the most widely used mode-locking strategy due to its desirable properties: short pulses, high frequency repetition rates and operation without a microwave oscillator. These advantages are achieved by introducing

a saturable absorber (SA), which works as a nonlinear absorption component in the cavity[22]. In integrated SMLLs, this function is generally realized by reverse biasing a section of the active region that is electrically isolated from the gain section (Fig. 2d). The SA section can be 'bleached' by an optical pulse with sufficiently high intensity to fill its conduction and valence bands with carriers, which suppresses further absorption. The pump level is chosen such that a continuous-wave (CW) optical field does not experience net gain due to the saturable loss, while a transient noise spike can bleach the saturable loss in the laser cavity to create a net gain window, preferentially leading to the build up of pulse oscillation[19]
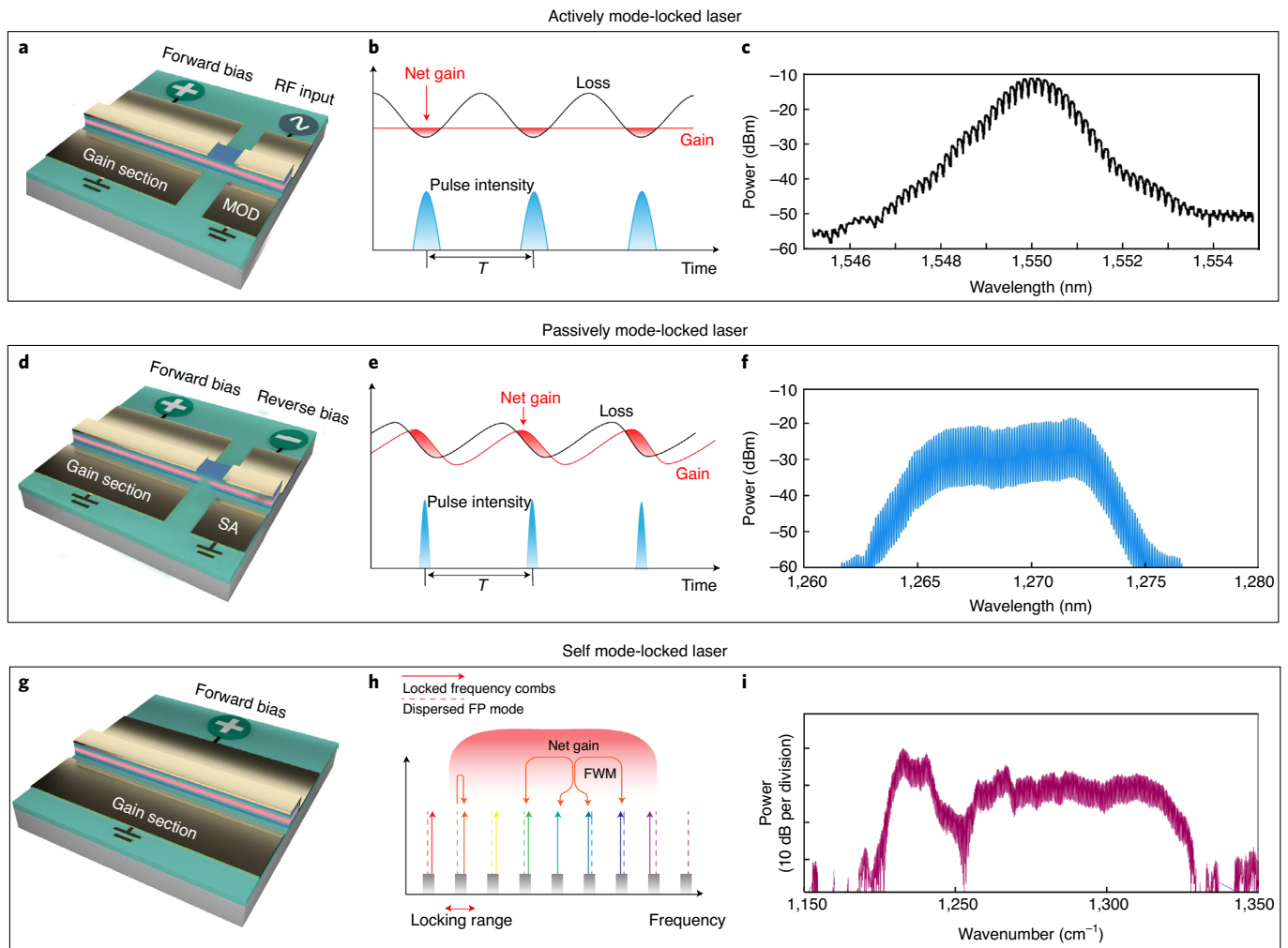
Fig. 2 | Integrated SMLL technologies. a, Schematic configuration of active mode locking. MOD, modulator. **b**, Loss and gain dynamics of active mode locking in the time domain. *T*, period. **c**, Representative active mode-locking spectrum (19.6 GHz) from an InP QW laser[21]. **d**, Schematic configuration of passive mode locking. **e**, Loss and gain dynamics of passive mode locking in the time domain. **f**, Representative passive mode-locking spectrum (20 GHz) from a GaAs QD laser[41]. **g**, Schematic configuration of self mode locking. **h**, FWM-assisted self mode-locking dynamics in the frequency domain. **i**, Representative self mode-locking spectrum (9.8 GHz) from a QCL[97]. Panels adapted with permission from: **c**, ref. [21], IEEE; **f**, ref. [41], OSA; **i**, ref. [97], American Institute of Physics.

(Fig. 2e). The gain section shortens the trailing edge of the pulse due to the gain saturation, while the SA section reduces the power in its leading edge, sharpening the pulse. Passive MLL technology can also be hybridized with active techniques by applying an RF signal to the reverse bias of the SA[23].

Generally, a passively mode-locked laser is said to be 'fundamental mode locking' when the SA section is close to one facet of the laser. In this case, only one pulse circulates in the cavity and the repetition rate is equal to the free spectral range (FSR) of the cavity. For a higher repetition rate (for example, >100 GHz), one must shorten the cavity length to increase the FSR, which can be undesirable as the gain from a shorter gain section may not be enough to overcome the overall loss. Colliding-pulse mode locking can address this issue by placing SA sections at specific integer fractions of the cavity length to realize a harmonic mode-locking operation. In harmonic mode locking, multiple pulses circulate in the cavity and pass through the SA section in colliding pairs that simultaneously saturate the absorber, enabling up to terahertz repetition rates in cavities with a much lower fundamental frequency[24]. An alternative method to realize a higher repetition frequency is to build a compound cavity to leverage the Vernier effect[25].

Self mode locking. Self mode locking is a phenomenon by which an OFC can be generated directly by a single-section laser structure without any active or passive modulation applied (Fig. 2g). This approach is appealing because the SA section of a typical passive MLL increases the intracavity loss, resulting in reduced power and efficiency. Self mode-locking behaviour is enabled by strong four-wave mixing (FWM) within the active medium combined with the spatial hole-burning effect[26–29] in a Fabry–Perot (FP) cavity (Fig. 2h). This effect generally exists in all types of MLLs, but is particularly important for quantum cascaded lasers (QCLs) where the ultrashort excited-state lifetime prevents passive mode locking. More recent findings have revealed that quantum cascade ring lasers, despite the absence of the spatial hole-burning effect, can still generate frequency combs induced by phase turbulence[30]. Notably, self MLLs usually exhibit superior coherence over comb lines[27], but they do not necessarily produce single pulses: while the modes of these devices are locked in the sense that they maintain a stable phase relationship, they might not share a uniform phase throughout the spectrum.

Material platforms. Integrated SMLLs were first demonstrated by using quantum well (QW) structures, where one-dimensional carrier

confinement led to overall performance improvements in the lasing thresholds, locking bandwidth and RF linewidth compared with bulk material systems[31]. QW material systems, including InGaN/GaN[32], AlGaAs/GaAs[33], InGaAsP/InP[34] and AlGaInAs/InP[35], have become the most widely used active media. With the advent of quantum dot (QD) material systems, such as InAs/GaAs[36] and InAs/InP[28,37], where carriers are confined in all three dimensions, even better MLL performance is expected[36,38]. Since QDs exhibit a delta-function-like density of states, an enhanced pulse-shaping mechanism in passive mode locking can be attained[36]. Such energy-band structures enable a higher population inversion efficiency, lower threshold current density and lower temperature sensitivity compared with QWs[39]. Furthermore, due to the random, self-assembled nature of QD formation, QD MLLs feature inhomogeneously broadened gain profiles and a near absence of gain competition, which is advantageous for broad bandwidth comb generation[40]. The effective carrier localization property in the QDs makes them less sensitive to growth defects, which enables high-quality QD-based MLLs to be grown epitaxially on silicon for MLLs[41].

Typical III–V QW and QD gain materials cover the wavelength range between 0.4 and 1.8 μm, while lasers at longer wavelengths often rely on interband cascade lasers (3–4 μm) or QCLs (>3 μm). For QCLs, it is challenging to realize the standard two-section passive MLL structures, due to a fast gain recovery (~0.3 ps)[27] that is much shorter than the cavity roundtrip time. Instead, active or self mode locking can be applied to enable combs for QCLs[42].

Integrated nonlinear optical frequency comb

Driven by an optical pump, nonlinear OFCs utilize the nonlinearities of optical media to generate comb lines. Based on the type of nonlinearity, they can be divided into three main classes: Kerr comb, electro-optic (EO) comb and quadratic comb. Even though the first integrated nonlinear OFCs[43,44] were made 20 years later than the first integrated SMLLs, the past decade has witnessed rapid progress in their development (Fig. 1, upper half). These recent advances hinge on the ability to strongly confine waveguide modes and precisely control the waveguide geometry in integrated photonics platforms. In addition to compactness and scalability, precision manufacturing provides chip-based nonlinear frequency combs with greater flexibility in design compared with earlier fibre- or nonlinear-crystal-based approaches.

Kerr comb. A Kerr comb is the most prevalent example of integrated nonlinear OFCs. Two major categories of Kerr combs are supercontinuum generation (SCG) in waveguides (Fig. 3a, upper part) and Kerr comb generation through microresonators (so called microcombs) (Fig. 3a, lower part). Since both processes originate from FWM via the third-order ($\chi^{(3)}$) nonlinear interactions (Fig. 3b), much of the underlying physics share similarities. We highlight the key features here and a more detailed discussion can be found in refs. [8,45].

For Kerr comb generation, useful coherent states usually take the form of solitons[46]—self-sustaining wavepackets in which all frequency comb lines are phase locked with each other. Soliton engineering requires manipulation of the dependence of refractive index on wavelength, that is, dispersion engineering (Fig. 3c), to achieve phase matching of the FWM process. In integrated photonics, a waveguide's dispersion can be engineered by tailoring its geometry. Appropriate design and fine fabrication control can create a broad anomalous dispersion window[47] and produce dispersive waves, resulting in a wide comb[48]. Kerr combs with octave-spanning OFCs have been realized in integrated photonics[49,50], facilitating essential f–$2f$ self-reference demonstrations[51].

Supercontinuum generation. The pump of an integrated supercontinuum consists of a train of ultrashort pulses, usually from an MLL

source. The pump light propagates through a nonlinear waveguide and undergoes spectral broadening. To preserve the coherence of the initial pulse train, the spectral growth needs to originate from self-phase modulation rather than noise amplified by modulation instability[52]. For this consideration, it is beneficial to use a waveguide with weak normal dispersion driven by short input pulses with a lower soliton number[53]. On the other hand, waveguides with anomalous dispersion offer a broader comb span[54]. Due to the high peak power, SCG is not usually driven by Kerr nonlinearity alone, but involves complex higher order processes. Detailed discussions can be found in ref. [55].

Kerr microcomb generation. The first mode-locked Kerr microcomb was achieved by incorporating a microresonator and an optical source within a fibre loop to form a ring laser[56], which is a configuration now called a 'laser cavity-soliton'. Today, the more widely used configuration is to drive a microresonator with an external CW pump: by simultaneously balancing dispersion against nonlinearity and loss against parametric gain, a microresonator in the anomalous group-velocity dispersion (GVD) regime can support fully mode-locked comb states called dissipative Kerr solitons (DKSs)[57]. To produce such low-noise combs, the pump laser is usually scanned into the cavity's resonance from blue to red (or the resonator is tuned from red to blue using heaters[58]), causing the spectral output to progress through primary sidebands and chaotic combs until it reaches the DKS regime[59]. Soliton formation occurs when the pump is red detuned from cavity resonances and the intracavity power is bistable. Thermal effects complicate this detuning procedure and therefore lead to non-trivial triggering and control protocols in soliton operation. Coherent comb states can also be generated by microresonators with normal GVD, which generate 'dark pulses' (short dips in the CW background)[60]. These dark-pulse mode-locked states usually result from perturbations of dispersion due to coupling between two mode families[60]. Since dark pulses exhibit desirable properties in conversion efficiency, comb power and operational simplicity, they have recently attracted remarkable research attention.

Another emerging Kerr comb generation approach is to drive a microresonator with a pulse input[59]. Such synthesis between conventional SCG and soliton microcombs takes equal advantage of the resonant enhancement offered by the cavity as well as the high peak power allowed by pulse pumping, therefore leading to both low threshold and high conversion efficiencies[61].

Material platforms. Due to the appealing properties of Kerr combs and the universal existence of $\chi^{(3)}$ in photonic materials, researchers have demonstrated Kerr combs in a number of integrated photonic platforms, including Si_3N_4 (ref. [62]), SiO_2 (ref. [63]), Hydex[64], Si[65], AlGaAs[66], AlN[67], GaP[68], $LiNbO_3$ (ref. [69]), Ta_2O_5 (ref. [70]), SiC[71], SiGe[72], diamond[73] and chalcogenide[74]. At present, Si_3N_4 is the most intensively studied and arguably the most mature platform, benefiting from a low material loss, a wide transparency window and a CMOS-compatible fabrication process[16]. AlGaAs is another promising material, with the highest nonlinear efficiencies among the materials mentioned here, and a quality (Q) factor that has dramatically improved over the past two years[75]. Materials with $\chi^{(2)}$ effects, such as $LiNbO_3$, AlGaAs, GaP, AlN and SiC, notably offer the potential to demonstrate octave-spanning Kerr combs and f–$2f$ interferometry in a single nonlinear medium[76].

Electro-optic comb. Another approach to generate OFCs employs the EO effect, the change of a material's refractive index under an electric field. Here we mainly focus on combs induced by the Pockels effect, where the change in refractive index depends linearly on the electric field. EO combs display unique advantages
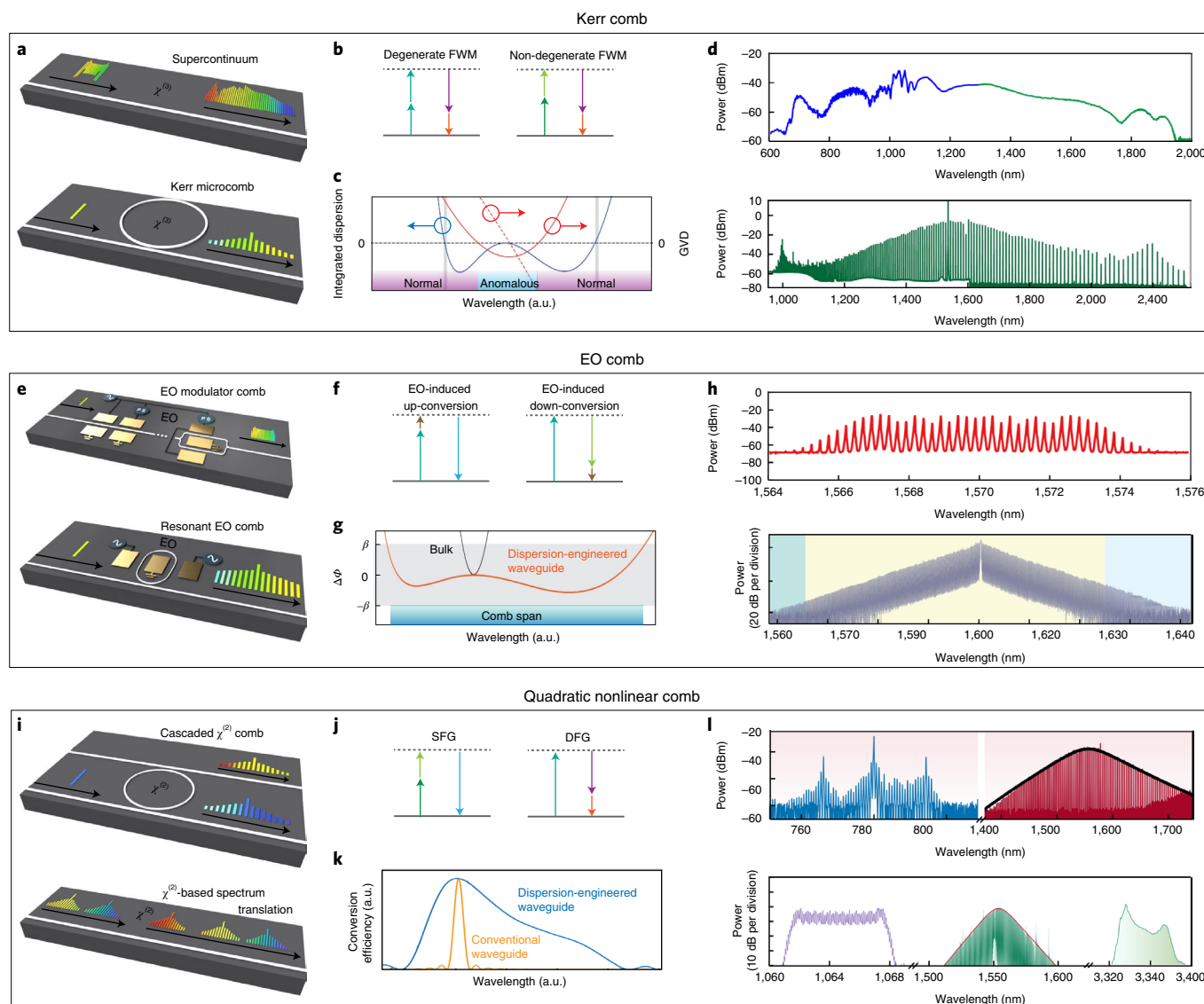
Fig. 3 | Integrated nonlinear OFC technologies. a, Schematic configurations of devices for SCG (upper part) and the Kerr microcomb (lower part).
b, Energy diagram of the FWM process for the Kerr comb, where arrows with different colors represent photons with different energies involved
in this process. **c**, Schematic drawing of dispersion engineering for the Kerr comb[8], where the GVD of the bulk material (dashed red line) and the
high-index-contrast waveguide (solid red line) are plotted. The GVD above/below zero corresponds to the normal/anomalous dispersion region. The
solid blue line represents the integrated dispersion of the waveguide. The grey-shaded lines where the integrated dispersion is zero indicate the location
of dispersive waves. **d**, Representative spectra for SCG (53 MHz) (upper)[54] and Kerr microcomb (1 THz) (lower)[50]. **e**, Schematic configurations of devices
for the EO modulator comb (upper part) and resonant EO comb (lower part). **f**, Energy diagram for the EO comb, where the brown arrow represents the
RF frequency and other colours are optical frequencies. **g**, Schematic drawing of the roundtrip phase ($\Delta\Phi$) versus the wavelength in bulk devices (black
line) and dispersion-engineered waveguides (orange lines) for the resonant EO comb[83]. The grey-shaded region shows the interference condition beyond
which the comb generation is suppressed, suggesting that dispersion engineering can significantly extend the comb span. β is the round-trip modulation
index. **h**, Representative spectra for the EO modulator comb (30 GHz) (upper)[78] and the resonant EO comb (10.453 GHz) (lower)[83]. **i**, Schematic
configurations of the cascaded $\chi^{(2)}$ comb (upper part) and $\chi^{(2)}$-based spectrum translation (lower part). In the cascaded $\chi^{(2)}$ comb, the pump light can
be either at the fundamental wavelength (yellow) or its SHG wavelength (blue), corresponding to different cascaded processes. **j**, Energy diagram of the
three-wave-mixing process for the quadratic comb. **k**, Schematic drawing of the transfer functions of the SHG process determined by the phase-matched
condition[15]. An integrated waveguide can enable a much broader bandwidth compared with bulk devices by simultaneously applying phase matching
and dispersion engineering. **l**, Representative spectra for the cascaded $\chi^{(2)}$ comb (361 GHz) (upper)[88] and the $\chi^{(2)}$-based spectrum translation (22 GHz)
(lower)[89]. Panels adapted with permission from: **c**, ref. [8], Springer Nature Ltd; **d**, refs. [54,50], OSA; **g**, ref. [83], Springer Nature Ltd; **h**, refs. [78,83], IEEE and Springer
Nature Ltd; **k**, ref. [15], OSA; **l**, refs. [88,89], Springer Nature Ltd and OSA.

in various scenarios, due to their reconfigurability and high
comb power. Developments over the past two years in integrated
EO combs suggest that novel integrated devices can potentially
address the bandwidth constraints and thus create new applica-
tion opportunities.

Electro-optic modulator comb. EO combs can be generated by pass-
ing a CW pump through modulators driven by RF sources[77] (Fig.
3e, upper part). The most straightforward way is to use a single
phase modulator. With current integrated LiNbO$_3$ modulators, this
method can generate up to 40 sidebands over a 10 nm span[78] (Fig. 3h,

upper plot). The intensity envelope of the spectrum follows a Bessel function, at whose nodes the comb line power can be very low. This problem can be addressed by cascading a series of phase modulators and one intensity modulator, which allows further phase tailoring to realize a shorter pulse and improved spectral broadening[77]. This strategy was developed a decade ago using bulk LiNbO$_3$ modulators in fibre optics and will likely be realized for integrated modulators in the near future.

Resonant electro-optic comb. Some early demonstrations of EO combs involved a modulator positioned inside an FP or fibre cavity, driven by an RF source whose repetition rate matches the FSR of the cavity; under these conditions, the resonance assists in sideband generation[79,80]. In integrated photonics, the resonant cavity is a microresonator with an internal phase modulator (Fig. 3e, lower part). The tight confinement of the waveguide enables more efficient modulation since the two electrodes can be placed only a few micrometres away[81]. More importantly, dispersion engineering allows constructive interference for cascaded frequency generation over a broader wavelength range[82] (Fig. 3g). When implemented with high-Q resonators, integrated EO combs can now cover the entire telecom C band with over 900 lines[83] (Fig. 3h, lower plot).

Material platforms. Since the Pockels effect is a second-order nonlinear property and therefore only appears in non-centrosymmetric crystals, suitable material platforms are scarcer than for Kerr processes. An attractive platform for integrated EO combs is lithium niobate-on-insulator (LNOI), which has become commercially available on high-quality wafers in the past few years. One key advance in LNOI is the reduction of waveguide propagation loss to as low as 3 dB m^{-1}, enabling resonator Q values of over ten million[84]. Other materials exhibiting EO effects, including AlGaAs, GaP, AlN and SiC, also have the potential to realize EO combs. Outside of the Pockels effect, modulators based on carrier-induced index change, such as Si or InP devices, can also be used to produce EO combs[85], but so far these mechanisms suffer from undesirable nonlinearity and high waveguide losses.

Quadratic comb. Frequency combs originating from a quadratic nonlinearity were theoretically predicated and experimentally observed two decades ago[86]. Since $\chi^{(2)}$ is usually a stronger effect than $\chi^{(3)}$, quadratic combs have an intrinsic advantage in efficiency compared with Kerr combs. To generate such combs with desirable spectra requires both dispersion engineering and phase-match engineering[15] (Fig. 3k), which dictates phase relations between interacting waves in three-wave-mixing processes.

The early experiments with quadratic combs were all performed using bulk nonlinear crystals. The implementation of quadratic combs in integrated photonics over the past two years has enriched the study of comb-formation dynamics and has exposed novel features by leveraging certain advantages of high-index-contrast waveguides.

Cascaded $\chi^{(2)}$ comb. A back-to-back three-wave-mixing process (Fig. 3j), either by second-harmonic generation/sum frequency generation (SHG/SFG) followed by optical parametric oscillation/differential frequency generation (OPO/DFG) or the reverse way, can exhibit $\chi^{(3)}$-like effects, such as self-phase modulation, cross-phase modulation and so on. Thus, combs can be produced from the quadratic nonlinearity alone (Fig. 3i, upper part). The effective nonlinear index of this process is determined by the material's second-order nonlinearity and the phase mismatch of frequency carriers, and is usually 1–2 orders of magnitude higher than a material's ordinary Kerr effect[87]. As a result, cascaded $\chi^{(2)}$ combs in integrated photonics, from either waveguide SCG[15] or microcomb generation[88] (Fig. 3l, upper plot), show efficiencies higher than DKS

devices. Moreover, such combs produce useful double OFCs around the fundamental and harmonic wavelengths; the dual-combs facilitate spectral broadening and can be used for f–$2f$ self-reference when their spectra overlap.

$\chi^{(2)}$-based comb translation. Three-wave-mixing processes can also be used to translate an existing comb to another spectral regime (Fig. 3i, lower part). At visible or mid-infrared wavelength ranges where regular approaches for generating comb sources are usually challenging, due to either strong material dispersion or high waveguide loss, translation provides a flexible way to enable comb formation. Starting from the well-developed combs at telecom bands, integrated SHG/DFG has been demonstrated for either up- or down-conversion of the initial comb[69,89] (Fig. 3l, lower plot).

Material platforms. As with EO combs, most integrated quadratic combs currently rely on LNOI (second-order nonlinear coefficient, $d_{33} \approx 27$ pm V^{-1}), particularly integrated periodically poled lithium niobate (PPLN) waveguides. One advantage of using PPLN is that the phase match and dispersion can be engineered independently through periodic poling and geometry tailoring, which is essential for attaining a high conversion efficiency and a large bandwidth at the same time (Fig. 3k). The AlGaAs-on-insulator (AlGaAsOI) ($d_{14} \approx 180$ pm V^{-1}) exhibits one order of magnitude higher efficiencies than PPLN in $\chi^{(2)}$ processes[90] and is therefore another promising candidate for achieving quadratic combs. Cascaded quadratic microcombs have recently been achieved in AlN ($d_{33} \approx 1$ pm V^{-1}) resonators[88], whose large bandgap is appealing for extending combs into short wavelengths. Interestingly, recent work has revealed that both Si[91] and Si$_3$N$_4$ (ref. [92]) can also exhibit $\chi^{(2)}$ effects under the influence of a d.c. electric field, which potentially can lead to quadratic combs in CMOS-compatible platforms.

Key metrics and properties

Integrated OFCs provide a versatile toolbox for diverse applications. The design of a comb source for a specific purpose benefits from careful consideration of both the type of comb and the specific design parameters; the different aspects of comb performance preclude a one-size-fits-all solution. Table 1 summarizes the metrics of OFCs that are available using existing approaches. These metrics, as well as some other essential properties, are discussed in detail below.

Repetition rate and comb span. The starting point for a comb design usually focuses on two factors: the repetition rate and the comb's spectral breadth. For most applications, the repetition rate of the comb needs to be low enough to interact with the electronics used for signal detection and processing, typically at RF frequencies of the order of tens of gigahertz or less. At the same time, in optical-frequency-counting applications (metrology), large comb spans, usually broader than one octave, are required for the self-reference process. Unfortunately, it is challenging to achieve both simultaneously. For a given span, a lower repetition rate means more comb lines must be generated, therefore imposing more stringent requirements on the conversion efficiency from the pump to the sideband lines. In resonator-based nonlinear OFCs, the problem is highlighted because the cavity has to be relatively long (at the millimetre-to-centimetre scale) to realize the RF repetition rate, which results in low resonant enhancement of the intracavity power, as well as small temporal overlap between the driving CW laser and soliton pulses in DKS generation.

A map summarizing the repetition rate and spectral coverage for current integrated comb technologies is shown in Fig. 4a. Integrated SMLLs have been demonstrated with FSR values down to the sub-gigahertz range[93], but the bandwidths of SMLLs are only within tens of nanometres, limited by material gain and intracavity dispersion. By contrast, integrated nonlinear OFCs can deliver

Table 1 | Summary of the key metrics of current integrated OFC technologies

Comb type	Pump type	Repetition rate	Comb span	Comb power	Pump power	Conversion efficiency	Optical linewidth /noise of comb lines	Microwave linewidth/noise
Active MLL	Electrical pump, RF input	Gigahertz to tens of gigahertz	Less than 10 nm	Up to milliwatt-level average comb power, tens of milliwatts peak power, sub-milliwatt power per line	Electrical power, hundreds of milliwatts d.c. power, high RF power	A few per cent	Hundreds of kilohertz to megahertz fundamental Lorentzian linewidth	Follow RF input
Passive MLL	Electrical pump	Sub-gigahertz to terahertz	Up to tens of nanometres	Up to tens of milliwatts average comb power, watt-level peak power, milliwatt-level power per line	Electrical power, hundreds of milliwatts	Up to 15% WPE	Hundreds of kilohertz to megahertz fundamental Lorentzian linewidth	Down to hertz-level linewidth, −115 dBc Hz⁻¹ at 100 kHz with external cavity
Self MLL	Electrical pump	Tens of gigahertz to hundreds of gigahertz	Up to tens of nanometres	Telecom band: up to tens of milliwatts average comb power, watt-level peak power, milliwatt-level power per line Mid-infrared: up to 1W	Electrical power, hundreds of milliwatts	Up to 10% WPE	Hundreds of kilohertz to megahertz fundamental Lorentzian linewidth	Down to hertz-level linewidth
Kerr comb — Supercontinuum	Pulse train	Megahertz to tens of gigahertz	Up to multi-octave span	Up to hundreds of milliwatts comb power, watt-level peak power	Optical power, hundreds of milliwatts comb power, watt-level peak power	Up to 60% optical conversion efficiency	Pump and broadening process determined	Follow pump
Microcomb bright soliton	CW laser	Gigahertz to terahertz	Up to one-octave span	Up to milliwatt-level comb power, sub-milliwatt power per line	Optical power, sub-milliwatt to hundreds of milliwatts level	Optical conversion efficiency < 5%	Pump noise dominate, tens of hertz fundamental Lorentzian linewidth achieved by injection locking	Down to −130 dBc Hz⁻¹ at 100 kHz noise
Microcomb dark pulse	CW laser	Gigahertz to terahertz	Up to hundreds of nanometres	Up to tens of milliwatts comb power, milliwatt-level power per line	Optical power, milliwatts to hundreds of milliwatts level	Up to 40% optical conversion efficiency	Pump noise dominate, hertz-level fundamental Lorentzian linewidth achieved by injection locking	Down to −140 dBc Hz⁻¹ at 100 kHz noise by self-injection locking
Pulse pumped microcomb	Pulse train	Gigahertz to tens of gigahertz	Up to hundreds of nanometres	Up to milliwatt-level comb power, sub-milliwatt power per line	Optical power, milliwatts to hundreds of milliwatts average power	Tens of per cent optical conversion efficiency	Pump and broadening process determined	Follow pump
EO comb — EO modulator comb	CW laser, RF input	Up to tens of gigahertz	Up to tens of nanometres	Microwatt-level power per line	Optical power flexible, high RF power	Optical conversion efficiency can be high, total conversion efficiency is low due to high RF power	Determined by pump noise and the multiplication of RF noise	Follow RF input
Resonant EO comb	CW laser, RF input	Up to tens of gigahertz	Up to 200 nm	Microwatt-level power per line	Optical power flexible, high RF power	Optical conversion efficiency < 5%, total conversion efficiency is low due to high RF power	Determined by pump noise and the multiplication of RF noise	Follow RF input
Quadratic comb — Cascaded $\chi^{(2)}$ supercontinuum	MLL	Megahertz to tens of gigahertz	Up to multi-octave span	Hundreds of milliwatts comb power, watt-level peak power	Optical power, hundreds of milliwatts comb power, watt-level peak power	Optical conversion efficiency up to 50%	Pump noise and broadening process determined	Follow pump
Cascaded $\chi^{(2)}$ microcomb	CW laser	Gigahertz to terahertz	Up to hundreds of nanometres	Comb power up to 20 mW	Optical power, hundreds of milliwatts	Optical conversion efficiency up to 20%	Pump noise determined	Pump and cavity determined
Comb translation	One or two combs	Pump comb determined	Up to tens of nanometres	Sub-milliwatt comb power	Optical power, hundreds of milliwatts	Optical conversion efficiency < 1 %	Pump noise determined	Follow pump

much broader nonlinear gains. At present, SCG is the most popular strategy for generating broad combs with detectable repetition rates. Multiple-octave spans, ranging from visible to mid-infrared wavelengths, have been achieved by both Kerr and quadratic SCG[14,15]. Dispersion engineering in Kerr microcombs has also produced combs from 1,000 to 2,400 nm (ref. [50]), but such combs have their FSR around 1 THz. Self-reference experiments with these devices rely on a second comb with a microwave repetition rate and whose comb spans only tens of nanometres[17,18,94]. Recent advances in pulsed driven microcombs can potentially bridge this gap with much higher conversion efficiencies by utilizing enhanced temporal overlap between the pump and the DKSs[59]. The high nonlinear coefficients and the dual-comb nature of quadratic combs provide another prospective solution to this problem.

Power and efficiency. In many applications, the key factor that determines a system's performance is the comb output power. For instance, in communications, an optical link often requires more than 1 mW power at each wavelength to attain a satisfactory bit error rate. However, integrated OFCs generally exhibit a lower total output power than integrated single-wavelength lasers, and this power must be shared across multiple comb lines. For integrated SMLLs, the reduced power is usually due to the incorporation of the SA section. State-of-the-art integrated SMLLs[95] at the C band emit an average output power of nearly 100 mW and tens of comb lines with a milliwatt-level power, where the maximum total WPE is beyond 10% (Fig. 4b). Self mode-locked QCLs without a SA section can attain up to a power of 1 W (refs. [96,97]). Optical nonlinear processes are usually less efficient than direct electrical pumping method and generate lower comb powers. Although the highest on-chip optical pump-to-comb conversion efficiencies can reach over 50% in SCGs (Fig. 4c), the power of the individual comb lines is usually below 100 μW (ref. [98]). The conversion efficiencies of single DKSs[99] are usually low (1–5%), but they can be significantly higher in multi-soliton states (particularly soliton crystals[100]) or when using pulse pumping. Dark pulses can enable a conversion efficiency of >20% and generate about ten comb lines with a power of 1 mW (ref. [101]). Recent efforts to leverage $\chi^{(2)}$ in quadratic combs could yield further improvements in efficiency and power[88]. Another strategy to generate a high-power comb is to use EO combs with cascaded modulators, but these combs usually have a limited bandwidth and require RF supporting circuitry, which significantly increases the total power consumption[78].

Optical and microwave noise. In high-precision measurements such as sensing and timekeeping, optical and microwave spectral purity can directly impact the performance of the system. For instance, a narrow-linewidth laser is used to probe and manipulate atomic transitions with long coherence times in optical atomic clocks, while a low-noise microwave oscillator plays key roles in frequency division and synthesizing output signals[102]. When discussing optical noise, it is important to distinguish between two types of 'linewidths' that appear in the literature: the fundamental Lorentzian linewidth represents the noise floor far from the carrier frequency, while the Gaussian linewidth is defined as the full-width-half-maximum of the optical field power spectral density profile—usually for noise in the low-frequency range only. In the discussion here, all the optical linewidths refer to the fundamental Lorentzian linewidth[103].

Integrated SMLLs generally exhibit optical fundamental Lorentzian linewidths similar to FP semiconductor lasers—in the range of hundreds of kilohertz (kHz) to megahertz (MHz), limited by spontaneous emission noise and intracavity losses[104]. Injection locking has been used to reduce the optical linewidth down to the kilohertz level, but this technique usually requires a fibre- or free-space-based external setup[105]. On the other hand, the optical noise of nonlinear OFCs is usually dominated by noise translated from the pump light; therefore, using commercial narrow-linewidth lasers, the generated comb lines can achieve linewidths at the kilohertz level. In non-resonant nonlinear OFCs, such as SCG and EO combs, the coherence between the pump and the generated comb lines may not be preserved, which can degrade the spectrum purity. For evaluating the coherence over comb lines, various techniques have been developed, usually relying on coherence beatnote spectroscopy referenced to either a second comb source or a single mode laser[106].

Low-noise microwave oscillators play a key role in microwave photonics applications, such as radar[107], signal processing[108] and time–frequency metrology[17,18]. Such a capability was previously limited to bulk MLLs. So far, optical noise in integrated SMLLs has limited their RF performance and has prevented them from serving as an adequate substitute. Using an external fibre cavity, the RF linewidth of a free-running integrated SMLL based on a purely III–V cavity has been reduced from the order of hundreds of kilohertz down to the sub-kilohertz level[109]. Recently, a heterogeneously integrated III–V-on-Si MLL with a centimetre-long low-loss passive section achieved a sub-kilohertz RF linewidth[93]. Purely passive, high-Q resonators in integrated nonlinear OFCs perform considerably better as microwave oscillators; Kerr microcombs have achieved hertz-level RF linewidths[110].

In the past few years, the integration of a laser and an ultra-high-Q microresonator has led to orders of magnitude reduction in both optical and microwave noise compared with regular-pumped OFCs[16,111] (Fig. 4d,e), as will be discussed in a later section.

Operation simplicity and reconfigurability. All integrated OFC applications can benefit from a straightforward and standardizable OFC operation protocol. For most integrated SMLLs, a comb can be initialized by simply turning the laser on with an appropriate gain current and SA bias (passive MLLs). Given suitable RF modulation inputs, active MLLs and EO combs can also be operated easily. To produce a coherent state in $\chi^{(2)}$ or $\chi^{(3)}$ microcombs, however, is usually more challenging; coherent states only exist within a certain detuning range of the pump frequency relative to the resonances of the cavities, and establishing those states therefore requires careful attention to the thermal instability caused by varying the intracavity power. Common pump schemes have required a series of complex laser-tuning-and control procedures to initiate and stabilize the soliton combs[112]. These procedures have been a major obstacle for the microcomb research community. Soliton crystals can alleviate this problem thanks to the moderate intracavity power change that accompanies a state transition[100]. A newly developed 'turnkey' self-injection locking approach can (Fig. 4f) enable the direct generation of a soliton microcomb via an intrinsic optical-locking mechanism that requires no tuning or control procedures[111].

Some applications, such as dual-comb-based optical spectroscopy and light detection and ranging (or LIDAR) systems, require OFCs that can be tuned in both the repetition rate and carrier frequency, ideally with a wide tuning range. At present, non-resonant-comb-generation approaches generally exhibit the best tunability. For cavity-based comb sources, SMLLs can be efficiently tuned up to several nanometres of carrier wavelength when operated at the C band. Repetition-rate tuning via carrier injection and temperature has yielded a tuning width of up to 1 GHz while operating around 40 GHz (ref. [113]). High-Q dielectric resonators for integrated nonlinear OFCs usually suffer from a limited tuning range due to their narrow resonance and the lack of efficient index-changing strategies. For a 100 GHz Si_3N_4 comb, the FSR can be varied by only a few megahertz, with gigahertz-level wavelength chirping[10]. Resonator EO combs have a better detuning tolerance and can produce a repetition-rate tuning range (Δ) of up to 100 MHz while operating around 10 GHz (ref. [83]) (Fig. 4g).
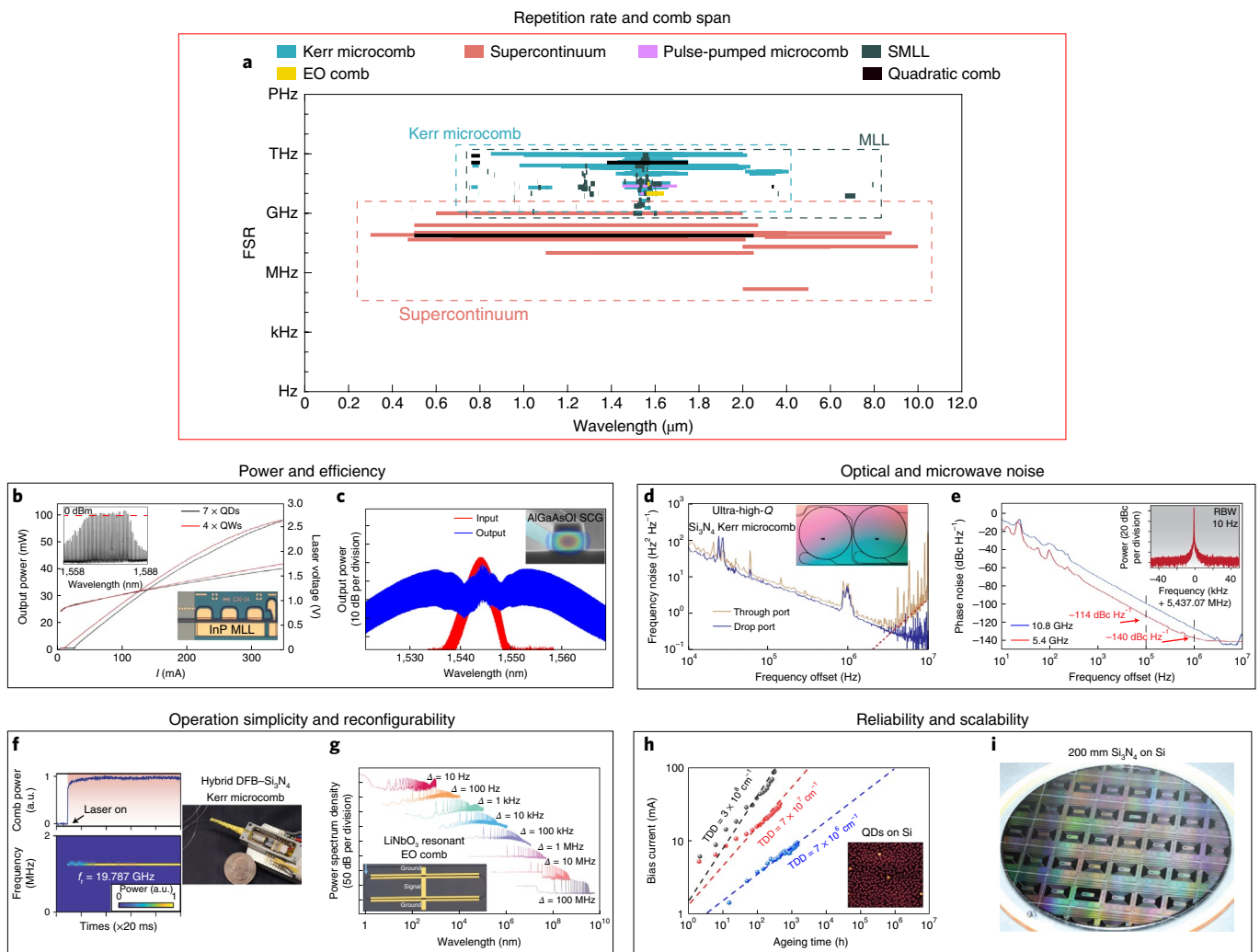
Fig. 4 | Current status of key metrics and properties of integrated OFC technologies. a, Map of the repetition rate and spectrum coverage for representative works using different comb-generation approaches (strips), where the three dashed boxes represent the expected coverages for the Kerr microcomb (blue), SCG (orange) and SMLL (dark green). Most of the references can be found in refs. [8,45,156]. **b**, Light–current–voltage testing results for high-power and high-efficiency InP MLLs and their spectra (inset at upper right)[95]. **c**, High-efficiency SCG using an AlGaAsOI waveguide (inset)[98]. Under 85 mW launched power (peak power ≈ 5.6 W) the optical pump-to-comb conversion efficiency is 66%. **d,e**, Ultra-low optical (**d**) and microwave (**e**) noise of combs enabled by the integration between a commercial DFB laser and an ultra-high-Q Si$_3$N$_4$ microresonator[16]. The optical carrier frequency is 192.7 THz. RBW, resolution bandwidth. **f**, Turnkey behaviour of integrated soliton microcombs by injection-locking a DFB laser into a Si$_3$N$_4$ microresonator (inset): measured comb power (top) and detected soliton repetition rate (f_r) signal (bottom) with the laser turn-on indicated at 10 ms (ref. [111]). **g**, Dual-tone LiNbO$_3$ resonant EO comb generation to highlight the reconfigurability of comb spacing, from 10 Hz to 100 MHz (ref. [83]). **h**, Lifetime testing results for QD lasers grown on silicon with a varying threading dislocation density (TDD)[115]. **i**, Photograph of a CMOS-foundry-produced 200-mm-diameter wafer for Kerr microcombs[16]. Panels adapted with permission from: **b**, ref. [95], OSA; **c**, ref. [98], Springer Nature Ltd; **d,e,i**, ref. [16], Springer Nature Ltd; **f**, ref. [111], Springer Nature Ltd; **g**, ref. [83], Springer Nature Ltd; **h**, ref. [115], American Institute of Physics.

Reliability and scalability. Although OFCs are already crucial for a variety of technologies, their use will be accelerated by high-volume, low-cost production in industry. Thanks to advances in semiconductor laser manufacturing, integrated SMLLs are currently closer to industry-scale use than other OFC technologies: various implementations of SMLLs have been successfully demonstrated in major commercial photonics platforms, including InP, GaAs and heterogeneous III–V on silicon-on-insulator (SOI). Recent breakthroughs with epitaxially grown QDs on Si suggest an economically viable way to integrate SMLLs with CMOS foundry processes[41,114]. Ageing tests of lasers on this platform have shown million-hour lifetimes at 80 °C (refs. [114,115]) (Fig. 4h), which can meet the stringent requirements of data centres and other demanding applications. On the other hand, similar studies for integrated nonlinear OFCs

are relatively sparse. Although passive optical devices tend to last much longer than SMLLs, nonlinear devices experience prolonged high light intensities, which may affect the material properties. In addition, without suitable mitigation, the high-Q cavities used in many nonlinear OFCs are usually influenced by various external factors such as the ambient air conditions, stress, temperature and pump-source considerations. Furthermore, any attempt to scale up the manufacturing of nonlinear OFCs must meet the precise waveguide-loss and geometry-control specifications for dispersion engineering and phase matching. Nevertheless, remarkable success has been achieved in adapting Kerr microcomb fabrication in CMOS lines[62,64]. Early efforts have been carried out by several companies providing dedicated wafer-scale processes for materials like Si$_3$N$_4$ (ref. [116]) and LiNbO$_3$ (ref. [117]), which are suitable for nonlinear

103

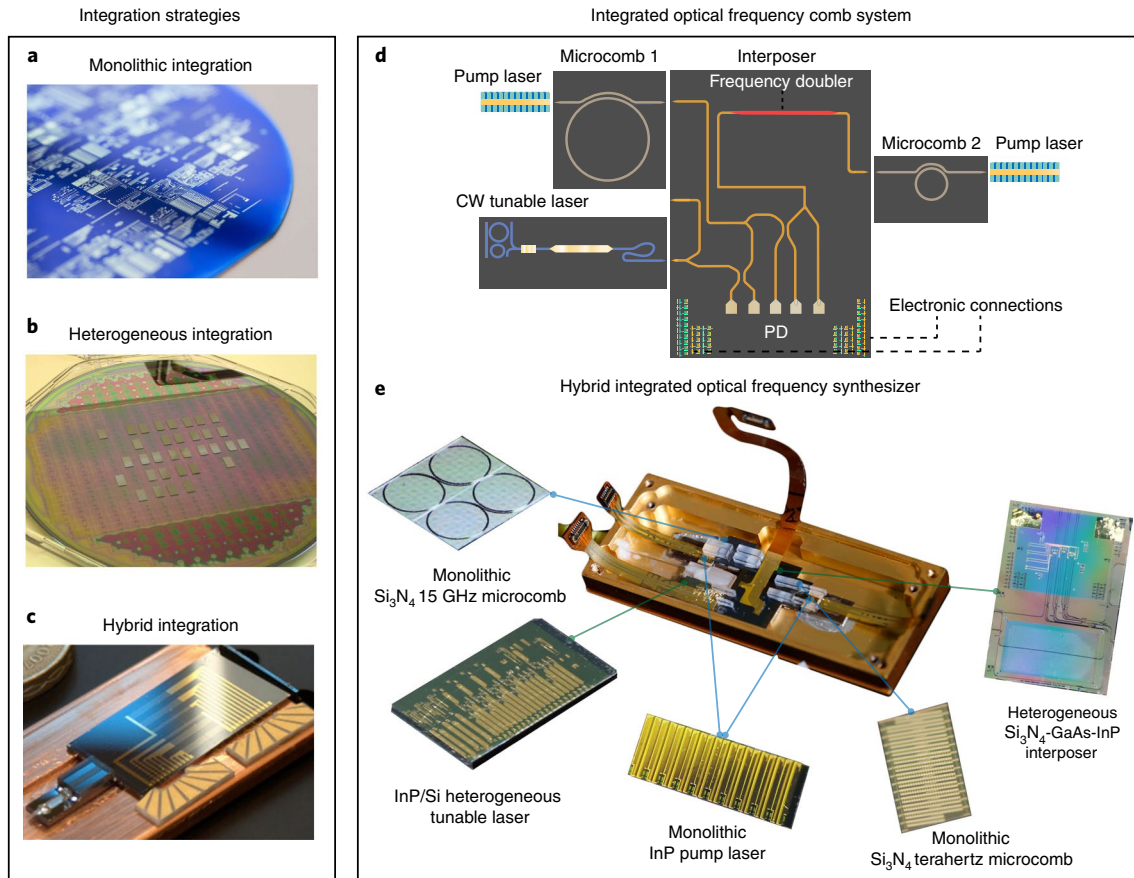**Fig. 5 | Current status of OFC integration in PICs. a–c**, Integration approaches of monolithic integration[118] (**a**); heterogeneous integration[120] (**b**) and hybrid integration[125] (**c**). **d**, Schematic of OFC-based optical frequency synthesizer system. PD, photodiode. **e**, Hybrid integrated optical frequency synthesizer system and all the individual photonic components realized by different integration strategies. Panels adapted with permission from: **a**, ref. [118], Novus Media Today Group; **b**, ref. [120], IEEE; **c**, ref. [125], American Institute of Physics.

purposes. One recent milestone resulting from these efforts is the Kerr microcomb in Si_3N_4 microresonators on standard 200 mm Si wafers from a CMOS foundry line[16] (Fig. 4i).

OFCs in photonic integrated circuits. Despite the phenomenal success of integrated OFCs at the device level, incorporating them into fully integrated photonic integrated circuits (PICs) remains elusive. In most integrated OFC demonstrations so far, the comb generators are the only components integrated on-chip. Hence, a large amount of bulk electronic and optical equipment is required for operating those systems, undermining practically all the benefits promised by integrated photonics. To dramatically reduce the system SWaP-C in commercial products, OFCs must be combined with at least a substantial portion of the photonic systems used in PICs. Here, we discuss the current status of high-level OFC integration with an eye towards further development.

Integration approaches. There are three important approaches to combining OFCs with other photonic components: monolithic, heterogeneous and hybrid techniques. Monolithic integration of multiple photonic devices has been widely deployed in large-scale foundry production[118] (Fig. 5a). Commonly used monolithic platforms in photonic foundries include InP and GaAs; these III–V semiconductors and epitaxial stacks of their alloys are grown at an industrial scale on native substrates. The high-quality QW and QD gain media that are available on those platforms naturally support integrated SMLLs and pump lasers for integrated nonlinear OFCs.

These light sources can then be joined to other active and passive components by intermixing or regrowth[119]. While active devices are well supported, the monolithic approach is less suitable for passive elements because of the relatively high waveguide losses and weak optical confinement. These issues have limited the scale-up and efficiency of monolithic III–V OFC PICs.

An alternative to monolithic PICs is heterogeneous integration, which leverages wafer-bonding or transfer-printing techniques to combine different material systems on the same wafer[120] (Fig. 5b) while maintaining the potential for wafer-scale processing[121]. In silicon photonics, heterogeneous integration has been used to transfer III–V materials onto silicon to unite electrically pumped lasers with low-loss waveguides and high-performance SOI passive devices[9]. Taking advantage of both materials, recent work has investigated III–V-on-Si MLLs with external SOI cavities as a means to overcome the linewidth bottleneck of pure III–V-based lasers[93]. Outside silicon photonics, a few novel nonlinear-medium-on-insulator platforms, such as LNOI[84] and (Al)GaAsOI[66], have been developed based on wafer-bonding technologies and used to produce integrated nonlinear OFCs. Furthermore, the recent demonstrations of a heterogeneous laser-soliton microcomb on silicon[122], enabled by III–V/Si/Si_3N_4 integration technology[123,124], paved the way towards integration of pump lasers and nonlinear media on the same wafer, which is expected to enable the mass production of integrated microcombs using photonic foundry processes in the near future. While heterogeneous integration offers large benefits over monolithic production, one drawback of processing diverse materials on

the same substrate is compatibility in fabrication, as in thermal budgets or etch steps.

In hybrid integration, fabrication restrictions are lifted by photonic-packaging techniques[125] (Fig. 5c). By combining chips after processing, these methods enable increased process independence[111,126,127], since the best devices can be selected beforehand to improve the yield compared with fully heterogeneous integration[128]. Those features are especially desirable for applications that demand fabrication-strict parts, for example, ultra-high-Q resonators whose performance can be degraded during multi-material processing. The commercial disadvantages of hybrid integration are cost and scalability. In addition, while the on-chip performance can be optimized, hybrid packaging processes result in lossier, less stable chip-to-chip and chip-to-fibre coupling. The higher reflections from those interfaces may affect laser operation, which could be potentially addressed by using QD lasers or a self-injection locking scheme.

High-level integration for SMLLs. The high-level integration of SMLLs has mainly been realized in monolithic III–V platforms. On InP, QW-based MLLs were successfully integrated on multi-project wafers alongside distributed Bragg reflectors, multimode interferometer couplers, phase modulators and semiconductor optical amplifiers (SOAs)—all fabricated via a generic foundry process[129]. In another study, an arrayed waveguide grating was implemented within a laser cavity to produce a multichannel harmonic MLL, which can potentially serve as a source for WDM communications[130]. Heterogeneously integrated SMLLs, however, have so far been produced only at the individual device level. We anticipate higher-level integration of heterogeneously fabricated MLLs in the near future, leveraging the mature process-development kit[9] component library of silicon photonics.

High-level integration for nonlinear OFCs. The crucial step for realizing nonlinear-OFC-based PICs is to connect the pump lasers with nonlinear devices. There were two considerable obstacles, but these can now be overcome. First, the pump power required for efficient comb generation was beyond the reach of integrated lasers in almost all nonlinear-OFC-generation approaches. Second, in the conventional pumping scheme, an optical isolator is required to protect the pump laser from feedback-induced interference, and such isolation is hard to realize in a PIC. Therefore, such laser–nonlinear-OFC integration was not possible until several recent breakthroughs. One key advance was the improvement in Q factors of microresonators, which enabled soliton generation for pump power at the milliwatt level in Si_3N_4 (ref. [110]) and AlGaAsOI[75] platforms. Regarding source-feedback issues, several strategies have been developed to circumvent the need for isolators by using new integrated photonic pumping schemes; one approach is to implement the nonlinear microresonators inside an external cavity coupled to the III–V gain section[127]. In that configuration, the resonator serves as both the comb generator and the reflector that provides feedback for lasing. Another recent approach that has been intensely studied is 'turnkey' self-injection locking of a pump laser via backscattering from a high-Q resonator[111,126,127]. This scheme enables a new operating regime for microcombs, where the soliton can be generated simply by turning on the laser power[111]. Such a turnkey operation eliminates the optical and electronic control circuitry, thereby dramatically reducing the microcomb system footprint and complexity. Another remarkable advantage of self-injection locking is the easing of dispersion requirements for Kerr comb generation. One milestone work[16] leveraging this technique is the generation of dark pulses in a thin-Si_3N_4, CMOS foundry platform that is directly pumped using a distributed feedback (DFB) laser. The resulting comb exhibited unprecedented low optical and microwave noise.

System-level applications. Several integrated photonic system demonstrations have been realized that make use of OFC devices in conjunction with other photonic components. An optical link has been reported that features an integrated SMLL, an SOA and silicon photonics transmitters and receivers packaged with supporting electronics chips; it supported a signal of 25 gigabits per second per comb line for dense wavelength division multiplexing (DWDM) communication[131]. In time–frequency metrology, one landmark study has reported an optical frequency synthesizer using a wide range of integrated photonic devices, including one 22 GHz SiO_2 comb, one 1 THz Si_3N_4 comb, a heterogeneously integrated III–V/silicon laser and one waveguide-based PPLN frequency doubler. This system generated a laser frequency output across 4 THz near 1,550 nm with 1 Hz resolution and 7.7×10^{-15} uncertainty[17]. In a subsequent generation, the integration level of this system was dramatically improved (Fig. 5d); both the microwave and terahertz soliton combs were generated using a Si_3N_4 resonator in a direct DFB-pumping manner. All the previously used fibre components were replaced by one Si_3N_4 interposer chip, where the AlGaAs doubler and InP QW photodiodes were heterogeneously integrated. Finally, all of the photonic chips were successfully packaged in a centimetre-scale assembly (Fig. 5e), connected to CMOS electronics chips through a flexible circuit board. Another demonstration has used a similar set of devices to realize an optical atomic clock by stabilizing the laser to an optical transition in a microfabricated rubidium vapour cell[18]. An interlocked frequency comb enabled the generation of an electronic 22 GHz clock signal with a fractional frequency instability of 10^{-13}. Although some bulk optics and electronics are still required in those systems, such proof-of-concept demonstrations show the promise of delivering integrated photonic solutions for high-level OFC-involved systems.

Challenges and outlook

Following the rapid research progress made in device development and system-prototype demonstrations, the field of integrated OFCs now stands at a critical point. On the one hand, the various comb-generation approaches have produced impressive figures of merit in device performances, many of which are comparable to bulk instrumentation, thus inviting many preliminary system-level applications. On the other hand, remarkable difficulties still exist and must be addressed to deliver the promised benefits of OFCs in PICs and ultimately transition this technology into commercial production.

One critical problem is the power. Although integrated SOAs could amplify the comb to power levels that are compatible with discrete lasers on-chip (milliwatts or higher), and which is compatible with current system applications of integrated photonics[131], they can only perform over a limited spectral bandwidth, usually less than tens of nanometres. Furthermore, amplification cannot improve the optical signal-to-noise ratio that is critical in optical networks. For the case of nonlinear OFCs, the pump power currently provided by integrated sources is still relatively low for octave-span generation, hindering applications that require self-referencing.

Another key challenge is the complexity of integrated OFC technologies, which impose more rigorous requirements on reliability, manufacturing and cost compared with previous PICs. For instance, replacing a sophisticated array of lasers in a WDM system with a single comb source may dramatically reduce the system SWaP-C, but the comb source must be proportionally more reliable and efficient. In addition, the rich dynamics behind comb formation often lead to multiple OFC states, adding significant instability during the operation. The required monitoring and control capabilities for comb operation present obstacles to full integration and deployment.

As such, a simplified, deterministic and reliable comb-operation protocol, with highly efficient comb-generation processes, will

essentially be the foundation of the whole integrated OFC technologies. Recent advances in the nanofabrication of diverse material platforms[75,110,123,132] and comb-generation schemes[100,111,133] suggest several promising solutions by combining high-quality devices with novel comb-formation dynamics. One example is the generation of soliton crystals in Kerr microcombs[100], which exhibit significantly higher efficiencies than the widely used single DKS and can be triggered by manual tuning. We also anticipate that harnessing the lower-loss cavities, the newly developed self-injection locking scheme[111] as well as the on-chip MLL stabilization[134], will play key roles since they can boost the efficiency of OFC generation and eliminate the need for tuning and control circuitry. Another exciting opportunity, which potentially can be offered by high-level integration, is the implementation of nonlinear devices inside the laser cavity, in the form of laser cavity-solitons[133], which may lead to high-efficiency, spontaneously formed combs by recycling the pump light.

Although a universal solution for comb generation that performs well in all aspects discussed in the 'Key metrics and properties' section would be ideal, in practice, integrated OFC deployment will mainly be application-driven. For communication use, integrated SMLLs with a repetition rate of less than 120 GHz will be used in photonic transceivers due to their advantages in comb power and efficiency as well as their compatibility with existing commercial photonic platforms. However, when data-rate requirements eventually push the comb span beyond the conventional telecommunications band, or demand extreme high-order quadrature amplitude modulation in coherent communications, the need for wide comb spectra and low noise will begin to favour microcombs. On the other hand, for timekeeping and frequency synthesis, Kerr combs will probably remain the predominate strategy in the foreseeable future due to their octave bandwidth that is required for self-referencing. In scenarios requiring greater reconfigurabilities, EO combs will probably play key roles. In the longer term, for systems of high complexity[17,18], multiple types of comb sources will co-exist and serve different purposes.

For commercial applications, the first widespread application for wafer-level-produced integrated OFC technologies will probably happen in DWDM photonic interconnects for data centres and high-performance computing. The integration of a comb source, photonic transceivers and microelectronics will enable data links with unprecedented bandwidth density, efficiency and reach[121]. The demands from industry will accelerate the adoption of OFC technologies in photonic foundries. Moving forwards, high-precision timekeeping and frequency synthesizing will embrace a massive market when integrated systems can maturely accommodate broader-span combs and attain higher-level complexity. Along the way, we do expect that integrated OFCs will find new markets in various important applications: the next generation of photonic neural network processor using microcomb parallelization holds promise in surpassing the speed and energy efficiency of cutting-edge graphics processing units[12,13]; the extension of OFCs to novel wavelength ranges, such as the visible region, could potentially bring new opportunities in areas like atomic physics and biosensing by integrated photonics, leveraging the recently developed CMOS-foundry-based visible photonic platform[135].

In just a few decades, integrated OFCs have overcome a number of difficult technical obstacles and have proved their viability as a means to support numerous invaluable integrated photonics technologies in a scalable fashion. With this rapid progress, we anticipate that the next decade will see implementations of OFCs in large-scale PICs, fuelling a new generation of emerging technologies in data transmission, sensing, timekeeping and fundamental science.

References

1. Hargrove, L. E., Fork, R. L. & Pollack, M. A. Locking of He–Ne laser modes induced by synchronous intracavity modulation. *Appl. Phys. Lett.* **5**, 4 (1964).
2. Diddams, S. A., Vahala, K. & Udem, T. Optical frequency combs: coherently uniting the electromagnetic spectrum. *Science* **369**, aay3676 (2020).
3. Marin-Palomo, P. et al. Microresonator-based solitons for massively parallel coherent optical communications. *Nature* **546**, 274–279 (2017).
4. Corcoran, B. et al. Ultra-dense optical data transmission over standard fibre with a single chip source. *Nat. Commun.* **11**, 2568 (2020).
5. Ye, J., Schnatz, H. & Hollberg, L. W. Optical frequency combs: from frequency metrology to optical phase control. *IEEE J. Sel. Top. Quantum Electron.* **9**, 1041–1058 (2003).
6. Fortier, T. & Baumann, E. 20 years of developments in optical frequency comb technology and applications. *Commun. Phys.* **2**, 153 (2019).
7. Beloy, K. et al. Frequency ratio measurements with 18-digit accuracy using a network of optical clocks. *Nature* **591**, 564–569 (2021).
8. Gaeta, A. L., Lipson, M. & Kippenberg, T. J. Photonic-chip-based frequency combs. *Nat. Photonics* **13**, 158–169 (2019).
9. Thomson, D. et al. Roadmap on silicon photonics. *J. Opt.* **18**, 073003 (2016).
10. Riemensberger, J. et al. Massively parallel coherent laser ranging using a soliton microcomb. *Nature* **581**, 164–170 (2020).
11. Wang, B. et al. Towards high-power, high-coherence, integrated photonic mmWave platform with microcavity solitons. *Light Sci. Appl.* **10**, 2047–7538 (2021).
12. Feldmann, J. et al. Parallel convolutional processing using an integrated photonic tensor core. *Nature* **589**, 52–58 (2021).
13. Xu, X. et al. 11 TOPS photonic convolutional accelerator for optical neural networks. *Nature* **589**, 44–51 (2021).
14. Carlson, D. R. et al. Photonic-chip supercontinuum with tailored spectra for counting optical frequencies. *Phys. Rev. Appl.* **8**, 014027 (2017).
15. Jankowski, M. et al. Ultrabroadband nonlinear optics in nanophotonic periodically poled lithium niobate waveguides. *Optica* **7**, 40–46 (2020).
16. Jin, W. et al. Hertz-linewidth semiconductor lasers using CMOS-ready ultra-high-Q microresonators. *Nat. Photonics* **15**, 346–353 (2021).
17. Spencer, D. T. et al. An optical-frequency synthesizer using integrated photonics. *Nature* **557**, 81–85 (2018).
18. Newman, Z. L. et al. Architecture for the photonic integration of an optical atomic clock. *Optica* **6**, 680–685 (2018).
19. Haus, H. A. Mode-locking of lasers. *IEEE J. Sel. Top. Quantum Electron.* **6**, 1173–1185 (2000).
20. Bowers, J. E., Morton, P. A., Mar, A. & Corzine, S. W. Actively mode-locked semiconductor lasers. *IEEE J. Quantum Electron.* **25**, 1426–1439 (1989).
21. Sato, K., Ishii, H., Kotaka, I., Kondo, Y. & Yamamoto, M. Frequency range extension of actively mode-locked lasers integrated with electroabsorption modulators using chirped gratings. *IEEE J. Sel. Top. Quantum Electron.* **3**, 250–255 (1997).
22. Derickson, D. J. et al. Short pulse generation using multisegment mode-locked semiconductor lasers. *IEEE J. Quantum Electron.* **28**, 2186–2202 (1992).
23. Liu, S. et al. Synchronized operation of a monolithically integrated AWG-based multichannel harmonically mode-locked laser. In *Proc. Optical Fiber Communication Conference* paper W4H.4 (Optical Society of America, 2016); https://doi.org/10.1364/OFC.2016.W4H.4
24. Chen, Y. K., Wu, M. C., Tanbun-Ek, T., Logan, R. A. & Chin, M. A. Subpicosecond monolithic colliding-pulse mode-locked multiple quantum well lasers. *Appl. Phys. Lett.* **58**, 1253–1255 (1991).
25. Kurczveil, G., Seyedi, M. A., Liang, D., Fiorentino, M. & Beausoleil, R. G. Error-free operation in a hybrid-silicon quantum dot comb laser. *IEEE Photonics Technol. Lett.* **30**, 71–74 (2018).
26. Liu, S. et al. 490 fs pulse generation from passively mode-locked single section quantum dot laser directly grown on on-axis GaP/Si. *Electron. Lett.* **54**, 432–433 (2018).
27. Hugi, A., Villares, G., Blaser, S., Liu, H. C. & Faist, J. Mid-infrared frequency comb based on a quantum cascade laser. *Nature* **492**, 229–233 (2012).
28. Lu, Z. G. et al. 312-fs pulse generation from a passive C-band InAs/InP quantum dot mode-locked laser. *Opt. Express* **16**, 10835–10840 (2008).
29. Khurgin, J. B., Dikmelik, Y., Hugi, A. & Faist, J. Coherent frequency combs produced by self frequency modulation in quantum cascade lasers. *Appl. Phys. Lett.* **104**, 081118 (2014).
30. Piccardo, M. et al. Frequency combs induced by phase turbulence. *Nature* **582**, 360–364 (2020).
31. Tucker, R. S. et al. 40 GHz active mode-locking in a 1.5 μm monolithic extended-cavity laser. *Electron. Lett.* **25**, 621–622 (1989).
32. Watanabe, H., Miyajima, T., Kuramoto, M., Ikeda, M. & Yokoyama, H. 10-W peak-power picosecond optical pulse generation from a triple section blue-violet self-pulsating laser diode. *Appl. Phys. Express* **3**, 52701 (2010).

33. Avrutin, E. A., Marsh, J. H. & Portnoi, E. L. Monolithic and multi-gigahertz mode-locked semiconductor lasers: constructions, experiments, models and applications. *IEE Proc. Optoelectron.* **147**, 251–278 (2000).

34. Williams, K. A., Thompson, M. G. & White, I. H. Long-wavelength monolithic mode-locked diode lasers. *New J. Phys.* **6**, 179 (2004).

35. Marsh, J. H. & Hou, L. Mode-locked laser diodes and their monolithic integration. *IEEE J. Sel. Top. Quantum Electron.* **23**, 1100611 (2017).

36. Thompson, M. G., Rae, A. R., Xia, M., Penty, R. V. & White, I. H. InGaAs quantum-dot mode-locked laser diodes. *IEEE J. Sel. Top. Quantum Electron.* **15**, 661–672 (2009).

37. Lelarge, F. et al. Recent advances on InAs/InP quantum dash based semiconductor lasers and optical amplifiers operating at 1.55 μm. *IEEE J. Sel. Top. Quantum Electron.* **13**, 111–123 (2007).

38. Rafailov, E. U., Cataluna, M. A. & Sibbett, W. Mode-locked quantum-dot lasers. *Nat. Photonics* **1**, 395–401 (2007).

39. Nishi, K., Takemasa, K., Sugawara, M. & Arakawa, Y. Development of quantum dot lasers for data-com and silicon photonics applications. *IEEE J. Sel. Top. Quantum Electron.* **23**, 1901007 (2017).

40. Bimberg, D. Quantum dot based nanophotonics and nanoelectronics. *Electron. Lett.* **44**, 168–171 (2008).

41. Liu, S. et al. High-channel-count 20 GHz passively mode-locked quantum dot laser directly grown on Si with 41 Tbit/s transmission capacity. *Optica* **6**, 128–134 (2019).

42. Wang, C. Y. et al. Mode-locked pulses from mid-infrared quantum cascade lasers. *Opt. Express* **17**, 12929–12943 (2009).

43. Del'Haye, P. et al. Optical frequency comb generation from a monolithic microresonator. *Nature* **450**, 1214–1217 (2007).

44. Hsieh, I.-W. et al. Supercontinuum generation in silicon photonic wires. *Opt. Express* **15**, 15242–15249 (2007).

45. Pasquazi, A. et al. Micro-combs: a novel generation of optical sources. *Phys. Rep.* **729**, 1–18 (2018).

46. Grelu, P. *Nonlinear Optical Cavity Dynamics. Nonlinear Optical Cavity Dynamics: From Microresonators to Fiber Lasers* (Wiley, 2016); https://doi.org/10.1002/9783527686476

47. Okawachi, Y. et al. Octave-spanning frequency comb generation in a silicon nitride chip. *Opt. Lett.* **36**, 3398–3400 (2011).

48. Brasch, V. et al. Photonic chip-based optical frequency comb using soliton Cherenkov radiation. *Science* **351**, 357–360 (2016).

49. Pfeiffer, M. H. P. et al. Octave-spanning dissipative Kerr soliton frequency combs in Si₃N₄ microresonators. *Optica* **4**, 684–691 (2017).

50. Li, Q. et al. Stably accessing octave-spanning microresonator frequency combs in the soliton regime. *Optica* **4**, 193–203 (2017).

51. Del'Haye, P. et al. Phase-coherent microwave-to-optical link with a self-referenced microcomb. *Nat. Photonics* **10**, 516–520 (2016).

52. Christensen, S., Ye, Z., Bache, M. & Company, V. T. Octave-spanning frequency comb generation in all-normal-dispersion silicon-rich silicon nitride waveguide. In *Proc. Conference on Lasers and Electro-Optics* paper STu3H.7 (Optical Society of America, 2020).

53. Sinobad, M. et al. Mid-infrared supercontinuum generation in silicon-germanium all-normal dispersion waveguides. *Opt. Lett.* **45**, 5008–5011 (2020).

54. Johnson, A. R. et al. Octave-spanning coherent supercontinuum generation in a silicon nitride waveguide. *Opt. Lett.* **40**, 5117–5120 (2015).

55. Dudley, J. M., Genty, G. & Coen, S. Supercontinuum generation in photonic crystal fiber. *Rev. Mod. Phys.* **78**, 1135–1184 (2006).

56. Peccianti, M. et al. Demonstration of a stable ultrafast laser based on a nonlinear microcavity. *Nat. Commun.* **3**, 765 (2012).

57. Kippenberg, T. J., Gaeta, A. L., Lipson, M. & Gorodetsky, M. L. Dissipative Kerr solitons in optical microresonators. *Science* **361**, eaan8083 (2018).

58. Joshi, C. et al. Thermally controlled comb generation and soliton modelocking in microresonators. *Opt. Lett.* **41**, 2565–2568 (2016).

59. Obrzud, E., Lecomte, S. & Herr, T. Temporal solitons in microresonators driven by optical pulses. *Nat. Photonics* **11**, 600–607 (2017).

60. Xue, X. et al. Mode-locked dark pulse Kerr combs in normal-dispersion microresonators. *Nat. Photonics* **9**, 594–600 (2015).

61. Weng, W. et al. Gain-switched semiconductor laser driven soliton microcombs. *Nat. Commun.* **12**, 1425 (2021).

62. Levy, J. S. et al. CMOS-compatible multiple-wavelength oscillator for on-chip optical interconnects. *Nat. Photonics* **4**, 37–40 (2010).

63. Li, J., Lee, H., Chen, T. & Vahala, K. J. Low-pump-power, low-phase-noise, and microwave to millimeter-wave repetition rate operation in microcombs. *Phys. Rev. Lett.* **109**, 233901 (2012).

64. Razzari, L. et al. CMOS-compatible integrated optical hyper-parametric oscillator. *Nat. Photonics* **4**, 41–45 (2010).

65. Griffith, A. G. et al. Silicon-chip mid-infrared frequency comb generation. *Nat. Commun.* **6**, 6299 (2015).

66. Pu, M., Ottaviano, L., Semenova, E. & Yvind, K. Efficient frequency comb generation in AlGaAs-on-insulator. *Optica* **3**, 823–826 (2016).

67. Jung, H., Xiong, C., Fong, K. Y., Zhang, X. & Tang, H. X. Optical frequency comb generation from aluminum nitride microring resonator. *Opt. Lett.* **38**, 2810–2813 (2013).

68. Wilson, D. J. et al. Integrated gallium phosphide nonlinear photonics. *Nat. Photonics* **14**, 57–62 (2020).

69. He, Y. et al. Self-starting bi-chromatic LiNbO₃ soliton microcomb. *Optica* **6**, 1138–1144 (2019).

70. Jung, H. et al. Kerr solitons with tantala ring resonators. In *Proc. Nonlinear Optics (NLO)* paper NW2A.3 (Optical Society of America, 2019).

71. Guidry, M. A. et al. Optical parametric oscillation in silicon carbide nanophotonics. *Optica* **7**, 1139–1142 (2020).

72. Ettabib, M. A. et al. Broadband telecom to mid-infrared supercontinuum generation in a dispersion-engineered silicon germanium waveguide. *Opt. Lett.* **40**, 4118–4121 (2015).

73. Hausmann, B. J. M., Bulu, I., Venkataraman, V., Deotare, P. & Lončar, M. Diamond nonlinear photonics. *Nat. Photonics* **8**, 369–374 (2014).

74. Gai, X., Madden, S., Choi, D.-Y., Bulla, D. & Luther-Davies, B. Dispersion engineered Ge₁₁.₅As₂₄Se₆₄.₅ nanowires with a nonlinear parameter of 136 W⁻¹ m⁻¹ at 1550nm. *Opt. Express* **18**, 18866–18874 (2010).

75. Chang, L. et al. Ultra-efficient frequency comb generation in AlGaAs-on-insulator microresonators. *Nat. Commun.* **11**, 1331 (2020).

76. Okawachi, Y. et al. Chip-based self-referencing using integrated lithium niobate waveguides. *Optica* **7**, 702–707 (2020).

77. Parriaux, A., Hammani, K. & Millot, G. Electro-optic frequency combs. *Adv. Opt. Photonics* **12**, 223–287 (2020).

78. Ren, T. et al. An integrated low-voltage broadband lithium niobate phase modulator. *IEEE Photonics Technol. Lett.* **31**, 889–892 (2019).

79. Kobayashi, T., Sueta, T., Cho, Y. & Matsuo, Y. High-repetition-rate optical pulse generator using a Fabry-Perot electro-optic modulator. *Appl. Phys. Lett.* **21**, 341–343 (1972).

80. Kourogi, M., Imai, K. & Widiyatomoko, B. Advances in electro-optic modulator based frequency combs. In *Digest of the LEOS Summer Topical Meetings, 2005* 133–134 (IEEE, 2005).

81. Wang, C. et al. Integrated lithium niobate electro-optic modulators operating at CMOS-compatible voltages. *Nature* **562**, 101–104 (2018).

82. Buscaino, B., Kahn, J. M., Lončar, M. & Zhang, M. Design of efficient resonator-enhanced electro-optic frequency comb generators. *J. Lightwave Technol.* **38**, 1400–1413 (2020).

83. Zhang, M. et al. Broadband electro-optic frequency comb generation in a lithium niobate microring resonator. *Nature* **568**, 373–377 (2019).

84. Zhang, M., Wang, C., Cheng, R., Shams-Ansari, A. & Lončar, M. Monolithic ultra-high-Q lithium niobate microring resonator. *Optica* **4**, 1536–1537 (2017).

85. Liu, S. et al. Microwave pulse generation with a silicon dual-parallel modulator. *J. Lightwave Technol.* **38**, 2134–2143 (2020).

86. Diddams, S. A., Ma, L.-S., Ye, J. & Hall, J. L. Broadband optical frequency comb generation with a phase-modulated parametric oscillator. *Opt. Lett.* **24**, 1747–1749 (1999).

87. Chang, L. et al. Second order nonlinear photonic integrated platforms for optical signal processing. *IEEE J. Sel. Top. Quantum Electron.* **27**, 5100111 (2020).

88. Bruch, A. W. et al. Pockels soliton microcomb. *Nat. Photonics* **15**, 21–27 (2020).

89. Bao, C. et al. Interleaved difference-frequency generation for microcomb spectral densification in the mid-infrared. *Optica* **7**, 309–315 (2020).

90. Chang, L. et al. Heterogeneously integrated GaAs waveguides on insulator for efficient frequency conversion. *Laser Photon. Rev.* **12**, 1800149 (2018).

91. Timurdogan, E., Poulton, C. V., Byrd, M. J. & Watts, M. R. Electric field-induced second-order nonlinear optical effects in silicon waveguides. *Nat. Photonics* **11**, 200–206 (2017).

92. Hickstein, D. D. et al. Self-organized nonlinear gratings for ultrafast nanophotonics. *Nat. Photonics* **13**, 494–499 (2019).

93. Wang, Z. et al. A III-V-on-Si ultra-dense comb laser. *Light Sci. Appl.* **6**, e16260 (2017).

94. Yi, X., Yang, Q.-F., Yang, K. Y., Suh, M.-G. & Vahala, K. Soliton frequency comb at microwave rates in a high-Q silica microresonator. *Optica* **2**, 1078–1085 (2015).

95. Zander, M. et al. High performance BH InAs/InP QD and InGaAsP/InP QW mode-locked lasers as comb and pulse sources. In *Proc. Optical Fiber Communication Conference* paper T3C.4 (Optical Society of America, 2020).

96. Lu, Q. Y., Manna, S., Slivken, S., Wu, D. H. & Razeghi, M. Dispersion compensated mid-infrared quantum cascade laser frequency comb with high power output. *AIP Adv.* **7**, 045313 (2017).

97. Jouy, P. et al. Dual comb operation of λ ∼ 8.2 μm quantum cascade laser frequency comb with 1 W optical power. *Appl. Phys. Lett.* **111**, 141102 (2017).

98. Hu, H. et al. Single-source chip-based frequency comb enabling extreme parallel data transmission. *Nat. Photonics* **12**, 469–473 (2018).

99. Bao, C. et al. Nonlinear conversion efficiency in Kerr frequency comb generation. *Opt. Lett.* **39**, 6126–6129 (2014).

100. Cole, D. C., Lamb, E. S., Del'Haye, P., Diddams, S. A. & Papp, S. B. Soliton crystals in Kerr resonators. *Nat. Photonics* **11**, 671–676 (2017).

101. Kim, B. Y. et al. Turn-key, high-efficiency Kerr comb source. *Opt. Lett.* **44**, 4475–4478 (2019).

102. Ludlow, A. D., Boyd, M. M., Ye, J., Peik, E. & Schmidt, P. O. Optical atomic clocks. *Rev. Mod. Phys.* **87**, 637–701 (2015).

103. Di Domenico, G., Schilt, S. & Thomann, P. Simple approach to the relation between laser frequency noise and laser line shape. *Appl. Opt.* **49**, 4801–4807 (2010).

104. Habruseva, T. et al. Optical linewidth of a passively mode-locked semiconductor laser. *Opt. Lett.* **34**, 3307–3309 (2009).

105. Lu, Z. G., Liu, J. R., Poole, P. J., Song, C. Y. & Chang, S. D. Ultra-narrow linewidth quantum dot coherent comb lasers with self-injection feedback locking. *Opt. Express* **26**, 11909–11914 (2018).

106. Burghoff, D. et al. Evaluating the coherence and time-domain profile of quantum cascade laser frequency combs. *Opt. Express* **23**, 1190–1202 (2015).

107. Xu, X. et al. Photonic microwave true time delays for phased array antennas using a 49 GHz FSR integrated optical micro-comb source [Invited]. *Photonics Res.* **6**, B30–B36 (2018).

108. Tan, M. et al. RF and microwave photonic temporal signal processing with Kerr micro-combs. *Adv. Phys. X* **6**, 1838946 (2021).

109. Haji, M. et al. High frequency optoelectronic oscillators based on the optical feedback of semiconductor mode-locked laser diodes. *Opt. Express* **20**, 3268–3274 (2012).

110. Liu, J. et al. Photonic microwave generation in the X- and K-band using integrated soliton microcombs. *Nat. Photonics* **14**, 486–491 (2020).

111. Shen, B. et al. Integrated turnkey soliton microcombs. *Nature* **582**, 365–369 (2020).

112. Yi, X., Yang, Q.-F., Youl Yang, K. & Vahala, K. Active capture and stabilization of temporal solitons in microresonators. *Opt. Lett.* **41**, 2037–2040 (2016).

113. Liu, H. F., Arahira, S., Kunii, T. & Ogawa, Y. Tuning characteristics of monolithic passively mode-locked distributed Bragg reflector semiconductor lasers. *IEEE J. Quantum Electron.* **32**, 1965–1975 (1996).

114. Shang, C. et al. High-temperature reliable quantum-dot lasers on Si with misfit and threading dislocation filters. *Optica* **8**, 749–754 (2021).

115. Norman, J. C., Jung, D., Wan, Y. & Bowers, J. E. Perspective: the future of quantum dot photonic integrated circuits. *APL Photonics* **3**, 030901 (2018).

116. Munoz, P. et al. Foundry developments toward silicon nitride photonics from visible to the mid-infrared. *IEEE J. Sel. Top. Quantum Electron.* **25**, 8200513 (2019).

117. Reimer, C. et al. Wafer-scale low-loss lithium niobate photonic integrated circuits. *Opt. Express* **28**, 24452–24458 (2020).

118. Advanced indium phosphide PDK for photonic integrated circuit design. *Novus Light Technologies Today* https://www.novuslight.com/advanced-indium-phosphide-pdk-for-photonic-integrated-circuit-design_N6729.html (2017).

119. Smit, M., van der Tol, J. & Hill, M. Moore's law in photonics. *Laser Photon. Rev.* **6**, 1–13 (2012).

120. Komljenovic, T. et al. Heterogeneous silicon photonic integrated circuits. *J. Lightwave Technol.* **34**, 20–35 (2015).

121. Margalit, N. et al. Perspective on the future of silicon photonics and electronics. *Appl. Phys. Lett.* **118**, 220501 (2021).

122. Xiang, C. et al. Laser soliton microcombs heterogeneously integrated on silicon. *Science* **373**, 99–103 (2021).

123. Xiang, C. et al. Narrow-linewidth III-V/Si/Si$_3$N$_4$ laser using multilayer heterogeneous integration. *Optica* **7**, 20–21 (2020).

124. Park, H., Zhang, C., Tran, M. A. & Komljenovic, T. Heterogeneous silicon nitride photonics. *Optica* **7**, 336–337 (2020).

125. Murray, E. et al. Quantum photonics hybrid integration platform. *Appl. Phys. Lett.* **107**, 171108 (2015).

126. Raja, A. S. et al. Electrically pumped photonic integrated soliton microcomb. *Nat. Commun.* **10**, 680 (2019).

127. Stern, B., Ji, X., Okawachi, Y., Gaeta, A. L. & Lipson, M. Battery-operated integrated frequency comb generator. *Nature* **562**, 401–405 (2018).

128. Carroll, L. et al. Photonic packaging: transforming silicon photonic integrated circuits into photonic devices. *Appl. Sci.* **6**, 426 (2016).

129. Guo, X., Quarterman, A. H., Wonfor, A., Penty, R. V. & White, I. H. Monolithically integrated tunable mode-locked laser diode source with individual pulse selection and post-amplification. *Opt. Lett.* **41**, 4835–4838 (2016).

130. Liu, S. et al. Synchronized 4 × 12 GHz hybrid harmonically mode-locked semiconductor laser based on AWG. *Opt. Express* **24**, 9734–9740 (2016).

131. Moscoso-Mártir, A. et al. Silicon photonics transmitter with SOA and semiconductor mode-locked laser. *Sci. Rep.* **7**, 13857 (2017).

132. Gong, Z., Liu, X., Xu, Y. & Tang, H. X. Near-octave lithium niobate soliton microcomb. *Optica* **7**, 1275–1278 (2020).

133. Bao, H. et al. Laser cavity-soliton microcombs. *Nat. Photonics* **13**, 384–389 (2019).

134. Srinivasan, S. et al. Hybrid silicon colliding-pulse mode-locked lasers with on-chip stabilization. *IEEE J. Sel. Top. Quantum Electron.* **21**, 1101106 (2015).

135. Morin, T. J. et al. CMOS-foundry-based blue and violet photonics. *Optica* **8**, 755–756 (2021).

136. Lee, H. et al. Chemically etched ultrahigh-Q wedge-resonator on a silicon chip. *Nat. Photonics* **6**, 369–373 (2012).

137. Herr, T. et al. Temporal solitons in optical microresonators. *Nat. Photonics* **8**, 145–152 (2014).

138. Brasch, V., Lucas, E., Jost, J. D., Geiselmann, M. & Kippenberg, T. J. Self-referenced photonic chip soliton Kerr frequency comb. *Light Sci. Appl.* **6**, e16202 (2017).

139. Rueda, A., Sedlmeir, F., Kumari, M., Leuchs, G. & Schwefel, H. G. L. Resonant electro-optic frequency comb. *Nature* **568**, 378–381 (2019).

140. Pfeifle, J. et al. Coherent terabit communications with microresonator Kerr frequency combs. *Nat. Photonics* **8**, 375–380 (2014).

141. Suh, M.-G., Yang, Q.-F., Yang, K. Y., Yi, X. & Vahala, K. J. Microresonator soliton dual-comb spectroscopy. *Science* **354**, 600–603 (2016).

142. Ho, P. -T., Glasser, L. A., Ippen, E. P. & Haus, H. A. Picosecond pulse generation with a cw GaAlAs laser diode. *Appl. Phys. Lett.* **33**, 241–242 (1978).

143. Huang, X. et al. Passive mode-locking in 1.3 µm two-section InAs quantum dot lasers. *Appl. Phys. Lett.* **78**, 2825–2827 (2001).

144. Koch, B. R., Fang, A. W., Cohen, O. & Bowers, J. E. Mode-locked silicon evanescent lasers. *Opt. Express* **15**, 11225–11233 (2007).

145. Morton, P. A. et al. Monolithic hybrid mode-locked 1.3 µm semiconductor lasers. *Appl. Phys. Lett.* **56**, 111–113 (1990).

146. Wu, M. C. et al. Transform-limited 1.4 ps optical pulses from a monolithic colliding-pulse mode-locked quantum well laser. *Appl. Phys. Lett.* **57**, 759–761 (1990).

147. Sato, K. 100 GHz optical pulse generation using Fabry-Perot laser under continuous wave operation. *Electron. Lett.* **37**, 763–764(1) (2001).

148. Meng, B. et al. Mid-infrared frequency comb from a ring quantum cascade laser. *Optica* **7**, 162–167 (2020).

149. Sato, K., Kotaka, I., Kondo, Y. & Yamamoto, M. Actively mode-locked strained-InGaAsP multiquantum-well lasers integrated with electroabsorption modulators and distributed Bragg reflectors. *IEEE J. Sel. Top. Quantum Electron.* **2**, 557–564 (1996).

150. Koch, B. R. et al. Monolithic mode-locked laser and optical amplifier for regenerative pulsed optical clock recovery. *IEEE Photonics Technol. Lett.* **19**, 641–643 (2007).

151. Tahvili, M. S. et al. Directional control of optical power in integrated InP/InGaAsP extended cavity mode-locked ring lasers. *Opt. Lett.* **36**, 2462–2464 (2011).

152. Guo, X. et al. Monolithically integrated selectable repetition-rate laser diode source of picosecond optical pulses. *Opt. Lett.* **39**, 4144–4147 (2014).

153. Villares, G. et al. On-chip dual-comb based on quantum cascade laser frequency combs. *Appl. Phys. Lett.* **107**, 251104 (2015).

154. Kemal, J. N. et al. Coherent WDM transmission using quantum-dash mode-locked laser diodes as multi-wavelength source and local oscillator. *Opt. Express* **27**, 31164–31175 (2019).

155. Van Gasse, K. et al. III-V-on-silicon mode-locked lasers with 1-GHz line spacing for dual-comb spectroscopy. In *Proc. Conference on Lasers and Electro-Optics* paper SF1G.5 (Optical Society of America, 2020).

156. Davenport, M. L., Liu, S. & Bowers, J. E. Integrated heterogeneous silicon/III-V mode-locked lasers. *Photonics Res.* **6**, 468–478 (2018).

Acknowledgements

Competing interests

J.E.B. is a shareholder in two silicon photonics companies, Quintessent and Nexus Photonics. The remaining authors declare no competing interests.

Additional information

Correspondence should be addressed to Lin Chang or John E. Bowers.

Peer review information *Nature Photonics* thanks David Moss and the other, anonymous, reviewer(s) for their contribution to the peer review of this work.

Reprints and permissions information is available at www.nature.com/reprints.

Publisher's note Springer Nature remains neutral with regard to jurisdictional claims in published maps and institutional affiliations.